

NUREG/CR-4321  
LA-10478-MS

RI

# **Full-Scale Measurements of Smoke Transport and Deposition in Ventilation System Ductwork**

R. A. Martin  
D. L. Fenton\*

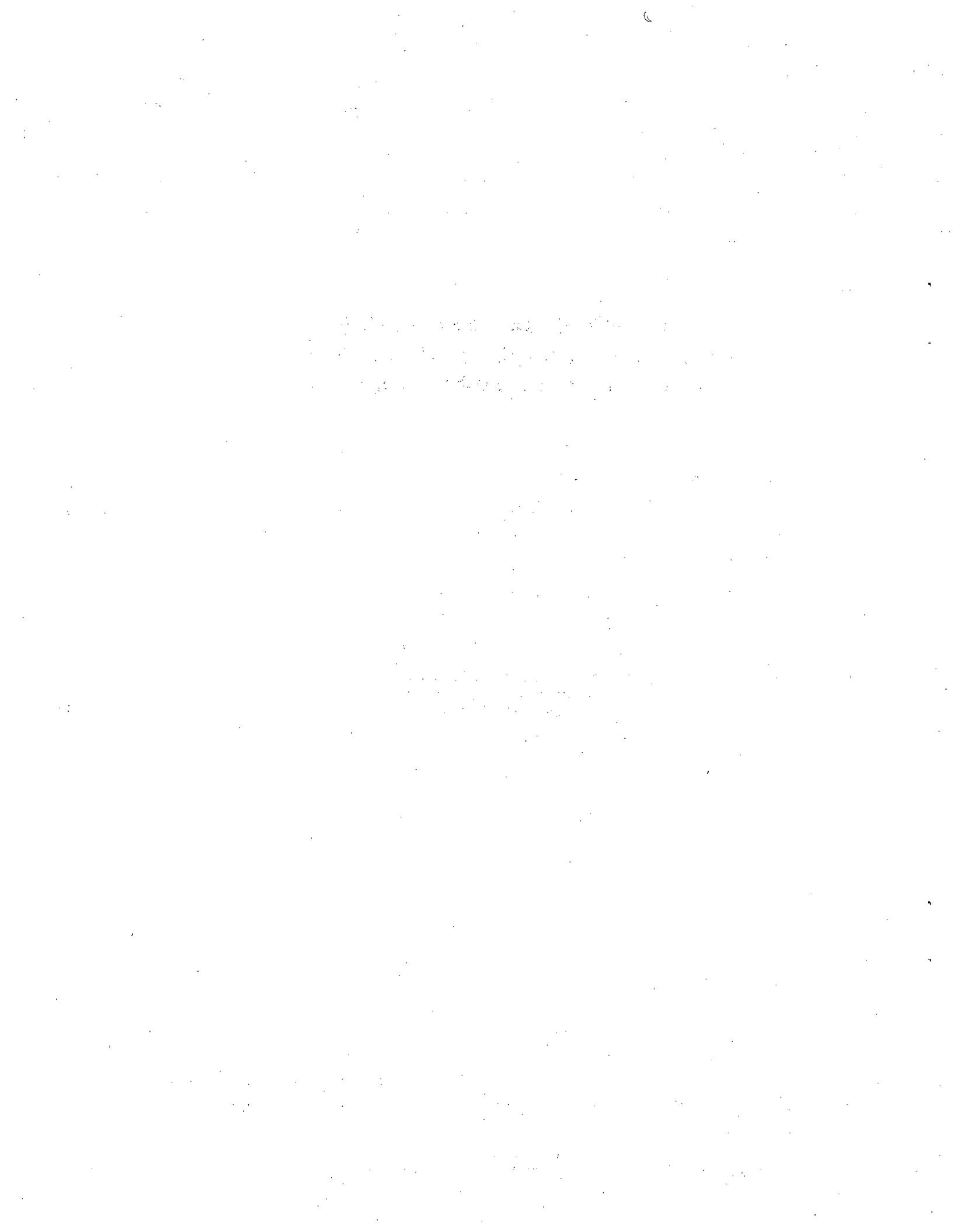
Manuscript submitted: June 1985  
Date published: July 1985

Prepared for  
Division of Risk Analysis  
Office of Nuclear Regulatory Research  
US Nuclear Regulatory Commission  
Washington, DC 20555

NRC FIN No. A7029

\*Consultant at Los Alamos. New Mexico State University, Las Cruces, NM 88003.

**Los Alamos** Los Alamos National Laboratory  
Los Alamos, New Mexico 87545



FULL-SCALE MEASUREMENTS OF SMOKE TRANSPORT  
AND DEPOSITION IN VENTILATION SYSTEM DUCTWORK

by

R. A. Martin and D. L. Fenton

ABSTRACT

This study is part of an effort to obtain experimental data in support of the fire accident analysis computer code FIRAC, which was developed at the Los Alamos National Laboratory. FIRAC can predict the transient movement of aerosolized or gaseous material throughout the complex ventilation systems of nuclear fuel cycle facilities. We conducted a preliminary set of full-scale material depletion/modification experiments to help assess the accuracy of the code's aerosol depletion model. Such tests were performed under realistic conditions using real combustion products in full-sized ducts at typical airflow rates. To produce a combustion aerosol, we burned both polystyrene and polymethyl methacrylate, the most and least smoky fuels typically found in fuel cycle plants, under varied ventilation (oxygen-lean and oxygen-rich) conditions.

Aerosol mass deposition, size, and concentration measurements were performed. We found that as much as ~25% of polystyrene smoke mass and as little as 2% of the polymethyl methacrylate generated at the entrance to a 15.2-m duct is deposited on the duct walls. We also compared our experimental results with theoretical equations currently used in FIRAC.

---

I. INTRODUCTION

A. Background

The Los Alamos National Laboratory is participating in a nuclear fuel cycle facility safety analysis program whose objective is to develop user-oriented tools for making better estimates of accident-induced radioactive aerosol release or source-term characteristics at a facility's atmospheric boundary.<sup>1,2</sup> These tools are intended to improve current safety analysis review techniques.

The plants being considered in this program include fuel fabrication, fuel re-processing, waste solidification, fuel storage, and  $UF_6$  production facilities. The types of accidents being considered include fires, explosions, spills, equipment failures, criticalities, and tornadoes.

Los Alamos developed the fire accident analysis computer code FIRAC to help evaluate the consequences of fire accidents in fuel cycle plants.<sup>3</sup> FIRAC was designed to predict transient fire-induced flows, temperatures, and material transport within facilities. FIRAC can model an interconnected network of rooms and typical ventilation system components such as ducts, fans, dampers, and protective high-efficiency particulate air (HEPA) filters.

The objective of the material transport portion of FIRAC is to estimate the movement of material (aerosol or gas) in an interconnected network of ventilation system components representing a given fuel cycle facility. Using this material transport capability, the code can calculate material concentrations and mass flow rates at any location in the network. Furthermore, the code will perform these transport calculations for various gas-dynamic transients. It solves the entire network for transient flow and in so doing takes into account system interactions.

A generalized treatment of material transport under fire-induced accident conditions could become very complex because several different types of materials could be transported. Also, more than one phase could be involved (including solids, liquids, and gases with phase transitions), and chemical reactions leading to the formation of new species could occur during transport. Further, for each type of material there will be a size distribution that varies with time and position depending on the relative importance of effects such as homogeneous nucleation, coagulation (material interaction), diffusion (both by Brownian motion and turbulence), and gravitational sedimentation. We know of no codes that can model transient flow-induced material transport in a network system subject to the possibility of all of these complications, and the transport portion of the FIRAC code does not include this level of generality either. However, this version of the code does provide a simple material transport capability. The material transport components of FIRAC consist of

1. material characteristics,
2. transport initiation,
3. convective transport,

4. aerosol depletion, and
5. filtration.

These components are described in more detail in Refs. 3--5. Here we are primarily concerned with item 4, aerosol depletion.

Although it can be thought that aerosol losses because of deposition (item 4) are insignificant, a previous study indicated that such losses can be appreciable in terms of mass percentage. Qualitative cascade impactor measurements in the downstream duct of full-sized compartment fire tests at Lawrence Livermore National Laboratory (LLNL) have indicated that as much as 60% of combustion product aerosol mass can be removed by deposition in a relatively short (~9.7-m-long) duct.<sup>6</sup> In case of a fire in a nuclear facility,<sup>3</sup> the presence of combustion products poses a threat to the HEPA filters.<sup>6--10</sup> A reduction in smoke concentration because of deposition can delay filter plugging. Because deposition depends on size,<sup>4</sup> it can modify the size distribution function of the smoke reaching the filters.

Further, in fuel cycle facilities under fire accident conditions, the smoke (solid and liquid aerosol) could be contaminated with radioactive material. In this case it becomes important to know where hazardous material is deposited and how much is deposited within the plant ventilation system. A reduction in airborne material concentrations will reduce the quantity of radioactive material accumulating on the HEPA filters and passing through them. We are particularly interested in the location and concentration of radioactive material in the respirable size range, namely, about 0 to 15  $\mu\text{m}$ . This time- and location-dependent concentration will change continually because of deposition and material interaction (coagulation).

Thus, there is a need to check the accuracy of the deposition equations available in the literature. Some of these deposition equations currently are being used to compute unsteady material depletion in FIRAC and other Los Alamos accident analysis computer codes.<sup>1,4</sup> The actual equations being used in FIRAC and suggested improvements to the code are discussed in Sec. II. However, such expressions have been confirmed only in small flow facilities using ideal aerosols. Thus, at this stage of computer code development, we have relatively little confidence in the predictions of deposition losses for combustion aerosols.

## B. Purpose of this Study

The current study is part of a Los Alamos effort to obtain experimental data in support of FIRAC computer code development and verification.<sup>1,3,7</sup> This study deals specifically with material transport area 4 listed above, aerosol depletion. Our purpose was to conduct a preliminary set of full-scale material depletion/modification experiments to obtain data on aerosol mass deposition, size, and concentration variations. In this study we performed such tests under realistic conditions using real combustion products (particulate and gaseous, including water vapor) in full-sized ducts at typical airflow rates. To produce a combustion aerosol we burned polystyrene (PS), and polymethyl methacrylate (PMMA), the most and least smoky fuels, respectively, typically found in nuclear fuel cycle facilities. We are unaware of adequate data of this kind in the available literature.

With such depletion/modification data we can help answer three questions for realistic fire conditions.

1. How important is deposition; that is, how much material accumulates on the walls?
2. How much change in smoke characteristics (concentration and size distribution) can occur over reasonable duct lengths?
3. Are our idealized equations from the literature giving us reasonable, and preferably conservative, quantitative estimates of deposition?

## C. Scope of the Study

A survey of combustible materials in fuel cycle facilities produced the typical fuel mixture composition given in Table I.<sup>2</sup> The composition percentages listed for these six materials represent a rough average for the facilities surveyed. They are likely to burn under both oxygen-rich and oxygen-starved (over- and under-ventilated) conditions to produce particulate material, water vapor, and gaseous combustion products.<sup>11</sup>

A special test facility was needed to obtain smoke deposition/modification data. We needed a facility in which some of the materials in Table I (or a mixture of materials) could be burned under controlled conditions so as to produce variable efficiencies. The burn products had to be introduced into as long a duct as practical to enhance deposition and aerosol concentration changes for better resolution. We also needed to simulate rapid diffusion (mixing) of the smoke plume to make an upstream, centerline smoke concentration measurement.

TABLE I  
TYPICAL FUEL MIXTURE COMPOSITION<sup>2</sup>

<u>Component</u>	<u>Composition (%)</u>
Polymethylmethacrylate	45
Cellulosic	26
Elastomer	18
Polyvinyl Chloride	8
Hydraulic Fluids	2
Polystyrene	1

Finally, we needed special experimental apparatus suitable for making surface measurements of total aerosol mass deposition.

A test facility was constructed by New Mexico State University (NMSU) and Los Alamos on the NMSU campus at Las Cruces, New Mexico. It had the dual purpose of allowing for the current studies and allowing for studies of HEPA filter plugging response to simulated fire accidents.<sup>7--9,12</sup> The facility described in Refs. 8 and 12 was modified to facilitate the current aerosol deposition/modification experiments. The major modifications included

1. coupling to a specially designed combustion chamber,
2. the design and installation of a biplanar grid of round tubes to promote turbulent mixing,
3. the construction of a metal hot duct, and
4. adding extra ductwork to bring the test section length for deposition up to ~15.24 m.

The proposed deposition/modification test series included a matrix of two pure materials (PS and PMMA) burned at two mass-burning (or smoke-generating) rates, high and low. The two materials were selected from Table I. Although PS is not found in as large proportions in nuclear fuel cycle facilities as is PMMA, PS is the most severe smoke producer in Table I. On the other hand, PMMA produces relatively low quantities of smoke per the amount of mass burned. Thus, by selecting these two fuels we attempted to bracket the extremes of smoke generation (the mass fraction of solid or liquid fuel that converts to smoke) expected in plants. For liquid PS and PMMA burned at over-ventilated conditions, Tewarson<sup>13</sup> experimentally measured smoke mass fractions ( $Y_s = m_s/m_b$ ) and got 0.33 and 0.021, respectively, where both the soot and low vapor pressure

liquids are included in the aerosolized combustion products or "smoke." The quantities  $m_s$  and  $m_b$  are mass of smoke produced and mass of fuel burned, respectively.

A special combustor was designed and manufactured by Battelle Pacific Northwest Laboratory (PNL) to burn the fuels and control the burning efficiency. The two mass burning rates were achieved by controlling the inlet air supply rate. Each burning rate was repeated two times for a total of four tests. The repetitions were used to assess the reproducibility of our test results. Appropriate instrumentation was set up and calibrated to obtain the following measurements.

1. Ambient pressure and temperature
2. Average or bulk volumetric airflow rate in the duct
3. Air temperature at four locations
4. Relative humidity
5. Fuel mass burning rate
6. Smoke mass concentration using cascade impactors at two locations on the duct centerline (downstream of the mixing grid and 13.9 m further downstream)
7. Smoke size distribution using eight-stage cascade impactors to obtain the mass median aerodynamic diameter and geometric standard deviation (for a log-normally distributed aerosol)
8. Total mass deposition at one downstream location but on three surfaces (ceiling, one side wall, and floor) at the 13.9 m downstream mass concentration measurement location (See item 6.)

We emphasize that the current study was useful but highly preliminary. Only a limited number of measurements have been made to date. Also, although much care was taken in the experimental procedures, relatively crude equipment was used to collect smoke deposits. Consequently, our deposition results must be viewed as qualitative. However, as we will discuss in Sec. IV, we believe that our deposition measurements are conservative and useful as such.

## II. AEROSOL DEPOSITION THEORY

### A. Existing FIRAC Capability

Because the flow Reynolds number will be greater than about 2100 for all cases of interest here (airflow in nuclear fuel cycle facilities), the flow always will be turbulent. We will assume that all flows are fully developed so that boundary layer or duct velocity profile shapes are constant with distance.

However, this will be true in most cases only sufficiently far downstream from the inlets (20 to 50 hydraulic diameters).

Under these conditions, not all of the material that is made airborne at the location of material transport initiation will survive convective transport to the filtration system's or facility's boundary. Depending on the aerosol aerodynamic characteristics and passage geometry, there may be a sizable reduction in aerosol concentration. As such, an enclosure or duct acts as an aerosol filter.

A user can calculate the aerosol losses caused by gravitational sedimentation in rooms, cells, and horizontal, rectangular ducts in the current version of FIRAC.<sup>3</sup> The deposition module can be turned on for horizontal ducts and rooms and turned off for vertical ducts by adjusting input flags. Aerosol depletion for any number of species and/or size distributions can be calculated throughout the network during transient flow. The theory is based on quasi-steady-state settling, with the terminal settling velocity corrected by the Cunningham slip factor. The flow in ducts and rooms is assumed to be well-mixed so that the aerosol concentration is uniform within the volume. More detail and references are discussed below. The user supplies only the aerosol diameter and density to this model. The aerosols may consist of solid particles or liquid droplets.

Future versions of the material transport module will account for combined molecular and turbulent diffusion as well as for aerosol interactions, but the current version is restricted to gravitational sedimentation. The particle flux  $J_p$  resulting from gravitational sedimentation is<sup>14</sup>

$$J_p = u_{ps} n_p, \quad (1)$$

where  $J_p$  is particles per unit area per unit time,  $u_{ps}$  is the terminal settling velocity, and  $n_p$  is the local aerosol number concentration in particles per unit volume for the homogeneous aerosol. If we multiply both sides of Eq. (1) by the homogeneous particulate mass  $m_p$  (assuming that we know this quantity or can calculate it from a measured aerosol size and mass density), then

$$J'_p = u_{ps} \rho_p', \quad (2)$$

where the units of  $J_p$  are mass per unit area per unit time and  $\rho_p = n_p m_p$  is the aerosol mass concentration per unit volume. The terminal settling velocity is calculated from<sup>14</sup>

$$u_{ps} = \frac{\rho_p d_p^2 g C}{18\mu} , \quad (3)$$

where

- $\rho_p$  = aerosol density,
- $d_p$  = aerosol particle diameter,
- $g$  = gravitational acceleration,
- $C$  = Cunningham slip correction factor, and
- $\mu$  = fluid dynamic viscosity.

The code input variables for material depletion are  $\rho_p$  and  $d_p$ . These variables may be assumed by the user. We recommend that the user select aerodynamic diameter with the unit density or Stokes diameter with the material bulk density. This selection was discussed earlier in this section. To calculate the slip correction factor, the code uses<sup>14</sup>

$$C = 1 + 2L/d_p \left[ A_1 + A_2 \exp(-A_3 D_p/L) \right] , \quad (4)$$

where  $L$  is the gas molecular mean free path and the  $A$ 's are dimensionless constants based on experimental measurements of small particle drag. The code uses

- $L = 0.065 \mu\text{m} ,$
- $A_1 = 1.257 ,$
- $A_2 = 0.400 ,$
- $A_3 = 0.550 ,$
- $g = 981 \text{ cm/s}^2 ,$  and
- $\mu = 0.0001781 \text{ g/cm-s} ,$

where  $L$ ,  $\mu$ , and  $g$  are taken at standard sea-level conditions.

We know  $\rho_p$  from the material transport mass balance calculation for the previous time step for each node (volume or duct). Then, knowing  $u_{ps}$  and the projected floor area for sedimentation  $A$ , we can compute the sink (or mass loss) term using Eq. (2),

$$\dot{m}_d = -J_p A = -u_{ps} \rho_p A, \quad (5)$$

which has the units grams per second. Because aerosol depletion is a sink term, we have used a minus sign in Eq. (5). Aerosol depletion by sedimentation may be selected for all volumes and ducts and is calculated in the same manner.

#### B. Future Improvements to FIRAC

Aerosols moving through passages that are horizontal (or not exactly vertical) can be deposited because of gravitational settling. However, a number of other processes that can cause aerosol depletion and contribute to a material transport sink term should be considered.<sup>14-20</sup> Particles that come sufficiently close to surfaces can be intercepted mechanically and stuck. Particles with enough inertia can deviate from the flow streamlines, impact, and stick to rough elements, obstacles, or bends. Particles less than about 1  $\mu\text{m}$  in size can be transported to surfaces by both turbulent (eddy) and molecular (Brownian) diffusion. Particles greater than about 1  $\mu\text{m}$  in size and being transported parallel to surfaces can be deposited because of the fluctuating velocity components normal to the surface (turbulent inertial deposition). Lower flow velocities enhance deposition caused by molecular diffusion and sedimentation. Unless the surfaces are sticky, the net rate of deposition will depend on the relative rates of transport and reentrainment. Except for fibrous particles or very light particles, interception may be neglected because particles large enough to be intercepted will most likely be deposited as a result of inertial effects or sedimentation.

Under certain conditions, other effects may become important for the smallest particles. These effects include thermophoresis, diffusiophoresis, and photophoresis migration, which are discussed in Refs. 14 and 17. They are believed to be relatively unimportant here compared with other effects.

Friedlander's book<sup>14</sup> provides an excellent introduction to deposition by convective diffusion and inertial deposition. Here the concept of a particle transfer coefficient  $k_p$  is introduced such that

$$J_p = k_p n_p \quad , \quad (6)$$

where  $J_p$  is the particle deposition flux (particles per square centimeter-second) at a given location in a tube and  $n_p$  is the local average particle number concentration (particles per cubic centimeter) in the mainstream at that cross section. Thus, the transfer coefficient  $k_p$  has units of centimeters per second and may be considered an effective deposition velocity. Experimental measurements of  $k_p$  for liquid droplets and solid particles were obtained for turbulent flow in vertical tubes at Reynolds numbers up to 50 000.<sup>21,22</sup> Several theories for predicting  $k_p$  for turbulent deposition are based on the diffusion free-flight model. Particles are assumed to be transported by turbulent diffusion to within one stopping distance from the wall, at which point the particles make a free flight to the wall. The stopping distance is

$$s_p = \bar{v}_p \tau_p = \rho_p d_p^2 \bar{v}_p / 18\mu \quad , \quad (7)$$

where  $\tau_p$  is the particle relaxation time and  $v_p$  is the assumed free-flight velocity.

Beal<sup>23</sup> has developed an analytical method for predicting  $k_p$  for turbulent flow in vertical tubes. Beal's method combines the approaches taken in Ref. 21 and Ref. 24 and applies them to particles ranging from molecular size to about 100  $\mu\text{m}$ . This theory accounts for the deposition mechanisms of Brownian and turbulent diffusion and turbulent inertial deposition but not gravitational settling. Beal's approach is to integrate the particle flux equation,

$$J_p = (D_p + \epsilon_p) \frac{dn_p}{dy} \quad , \quad (8)$$

across the concentration boundary layer. Here  $D_p$  is the particle coefficient of molecular diffusion and  $\epsilon_p$  is the particle eddy diffusivity (both have units of square centimeters per second). In the derivative,  $y$  represents distance in centimeters perpendicular to the surface. In his paper, Beal<sup>23</sup> states his assumptions for  $D_p$  and  $\epsilon_p$  in specific regions of the turbulent boundary layer and derives equations for  $k_p$ .

The authors of Ref. 25 have developed a method for predicting  $k_p$  for turbulent flow in horizontal tubes. This method applies to particles with a size greater than about 1  $\mu\text{m}$  because it accounts for the deposition mechanisms of turbulent diffusion and gravitational settling but does not account for Brownian diffusion. Reference 25 also considers the effect of pipe wall roughness and provides experimental verification for particles with sizes from about 1 to 4  $\mu\text{m}$ .

The equations for  $k_p$  presented in Refs. 23 and 25 were incorporated into a computer code called DUCT<sup>8</sup> that estimates aerosol depletion under steady flow conditions in a given duct segment. We propose to include these equations as an improvement to the aerosol depletion modules in the Los Alamos tornado and explosion accident analysis codes TORAC<sup>26</sup> and EXPAC,<sup>27</sup> respectively, as well as FIRAC.<sup>3</sup> (See also Refs. 1 and 4.)

Experimental data are needed to check aerosol depletion calculations for losses encountered in fuel cycle facilities, particularly for fire conditions, and such data are being sought in the current fuel cycle safety program. Another area needing improvement is accounting for the effects of other ventilation system components (besides filters) on aerosol removal. The other components include blowers, dampers, bends, and flow restrictions.

### C. Calculation of Integrated Material Losses Because of Sedimentation in a Duct

Equation (1) predicts the local flux of particles falling onto a horizontal unit surface area per unit time. We use the term "local" because to use Eq. (1) (in principle), we must know the aerosol concentration close to the surface. This local concentration of aerosol supplies particles for deposition. This is not a serious problem because turbulence effectively mixes the aerosol at a given duct cross-section except for a relatively thin (but important) region near the duct walls.<sup>14</sup> We also use the term local to remind ourselves that the aerosol concentration can change in the streamwise direction as well as in the transverse directions at a given duct cross-section. Further, to use Eq. (3)

to calculate the sedimentation transfer coefficient (settling velocity)  $u_{ps}$ , we must assume either that our aerosol is monodisperse ( $d_p = \text{constant}$ ) and homogeneous ( $\rho_p = \text{constant}$ ) or that our real aerosol can be adequately characterized by its median aerodynamic equivalent size (even though some variation in size and density exists from particle to particle). We have measured the mass median aerodynamic diameter (MMAD) of smoke using cascade impactors and found that the proper value of density for us to use in Eq. (3) is  $\rho_p = 1.0 \text{ g/cm}^3$ . (See Ref. 19.)

How can we calculate the total loss of aerosol material because of deposition that occurs from the inlet to the exit of a duct? For steady-state conditions, we expect this loss to be a function of the volume of aerosol-laden air that moves through the duct and the difference in concentration from inlet to outlet in a given time interval. Thus, by conservation of mass (or conservation of number of particles) we expect

$$N_p = (\text{particles in}) - (\text{particles out}) \quad , \quad (9)$$

where  $N_p$  is the total number of particles left behind in the duct (a loss, or sink, term). Equation (9) may be written as

$$N_p = N_{p0}Q\Delta t - n_pQ\Delta t = (n_{p0} - n_p)Q\Delta t \quad , \quad (10a)$$

where  $n_{p0}$  and  $n_p$  are the duct upstream (at the source) and downstream particle number concentrations, respectively;  $Q$  is the constant air volumetric flow rate; and  $\Delta t$  is the time interval over which deposition takes place. We assume that  $n_{p0}$  is greater than  $n_p$ .

For clarity, we will develop the simple expression for the concentration ratio,  $n_p/n_{p0} = \rho_p/\rho_{p0}$ , corresponding to deposition from an aerosol moving in a rectangular duct. This equation is given and discussed in Refs. 17 and 28. However, we follow the reasoning given by Fuchs<sup>15</sup> to derive the equation for a duct with a circular cross section. Consider an aerosol flowing in a con-

stant-area rectangular duct of height  $h$  and width  $w$  and assume that we know enough about the aerosol and the flow properties to calculate  $u_{ps}$  using Eq. (3). Assume further that the airflow is fully developed and turbulent and moves at bulk velocity  $U$ . Finally, assume that downstream distance is measured in  $x$  direction with  $n_p = n_{p0}$  given at  $x = 0$ . We are interested in calculating  $n$  at a downstream location  $x = L$ .

Our attention now is focused on a segment of duct of length  $\Delta x$  with cross-sectional dimensions  $w$  by  $h$ . The projected area for vertical settling of particles in  $\Delta x$  is  $w\Delta x$ . We also know that the well-mixed volume of aerosol-laden air in the segment is  $hw\Delta x$ . Therefore, using Eq. (1), the number of particles depositing onto area  $w\Delta x$  in time  $\Delta t = \Delta x/U$  is using Eq. (2)

$$\Delta N_p = J_p (\text{area})(\Delta t) = n_p u_{ps} (w\Delta x)(\Delta x/U) \quad (10b)$$

If we let  $\Delta n_p$  be the incremental change in concentration of particles per unit volume of air in the segment, then

$$\Delta n_p + \Delta N_p / hw\Delta x = n_p u_{ps} w (\Delta x)^2 / hw\Delta x U$$

Because  $\Delta n_p = n_{p2} - n_{p1} < 0$  for  $\Delta x = x_2 - x_1 > 0$ , we can write

$$-\Delta n_p / \Delta x = n_p u_{ps} / Uh$$

or, in differential form (in the limit as  $\Delta x$  goes to zero),

$$dn_p / dx = -n_p u_{ps} / Uh \quad (11)$$

This is a simple first-order ordinary differential equation for the variation of  $n$  with  $x$ . The known boundary condition is  $n_p = n_{p0}$  when  $x = 0$ . Separating the variables in Eq. (11) we get

$$dn_p/n_p = -(u_{ps}/Uh) dx .$$

Integrating using the dummy variables  $n'_p$  and  $x'$ , we have

$$\int_{n_{p0}}^{n_p} \frac{dn'_p}{n'_p} = \int_0^x - (u_{ps}/Uh) dx' ,$$

so

$$\ln \frac{n_p}{n_{p0}} = -u_{ps}x'/Uh \Big|_0^x ,$$

and

$$\ln (n_p/n_{p0}) = -u_{ps}x/Uh .$$

Finally,

$$\ln n_p/n_{p0} = e^{-(u_{ps}x/Uh)} . \quad (12)$$

Equation (12) gives the reduction in number concentration from  $n_{p0}$  to  $n_p$  in distance  $x$  down the duct. Thus, for constant, known values of  $u_{ps}$ ,  $h$ , and  $U$ ,

the concentration falls off exponentially from its initial values. Notice from Eq. (12) that increasing  $u_{ps}$  and  $x$  will enhance sedimentation, as will decreasing  $U$  and  $h$ .

As we can now calculate the local concentration  $n_p$  at  $x$  from Eq. (12), we can calculate the deposition flux at  $x$  using Eq. (1) to be

$$J_p = u_{ps} n_p = u_{ps} n_{po} e^{-(u_{ps} x / Uh)} \quad (13)$$

Using Eq. (13) we can calculate the integrated or total particulate deposition rate (in units of particles/s) up to  $x = L$  as

$$J_{ptot} A = \int_0^L J_p w dx = \int_0^L u_{ps} n_{po} e^{-(u_{ps} x / Uh)} w dx = n_{po} hwU \left[ 1 - e^{-(u_{ps} L / Uh)} \right] \quad (14)$$

where  $A$  is the duct floor area.  $Q = hwU$  is the duct flow rate in Eq. (14), and  $n_{po} Q = n_{po} hwU$  is the aerosol source strength in units of particles per second. For a time interval  $\Delta t$ , the total number of particles deposited in the duct may be calculated using Eqs. (14) and (12) and will be

$$\bar{N}_p = J_{ptot} A \Delta t = (n_{po} - n_p) Q \Delta t \quad (15)$$

Equation (15) gives the same result as Eq. (10), which followed from our heuristic thinking. For homogeneous particles of mass  $m_p$ , Eq. (15) gives the total mass deposition,

$$m_d = m_p \bar{N}_p = (\rho_{po} - \rho_p) Q \Delta t \quad (16)$$

and Eq. (12) gives the mass concentration ratio,

$$\rho_p' / \rho_{p0}' = e^{-(u_{ps} x / U_h)} \quad , \quad (17)$$

for any streamwise duct location  $x$ .

The FIRAC code makes a numerical approximation to the reduction in concentration because of sedimentation by using Eq. (5) directly if the duct lengths and computational time increments are sufficiently small. However, for longer ducts and/or sufficiently large or heavy materials (high  $u_{ps}$ ) for which concentration changes could exceed about 10% per time step, FIRAC can use Eq. (16) and Eq. (17) in combination. See Refs. 3--5 for more information on FIRAC material transport calculations.

### III. EXPERIMENTAL APPARATUS

The existing HEPA filter loading facility was modified to accommodate the requirements associated with combustion aerosol generation and deposition and filter plugging. The original filter loading facility is described in Ref. 8 and Ref. 12. Specifically, the modifications included the addition of approximately 7.4 m of straight duct upstream from the test filter location. The experimental apparatus consisted of the air handling equipment and associated instrumentation for characterizing the combustion products and smoke transport, and special apparatus for measuring smoke deposition in the duct.

#### A. Air Handling Equipment

The airflow equipment is shown in Fig. 1, which also gives the dimensions at the air supply and test section ends of the system. The distance from the burner inlet to the upstream side of the test section was 20.3 m. The maximum volumetric airflow rate through the system was 2040 m<sup>3</sup>/h. The wood ducts were constructed from 1.9-cm-thick plywood and reinforced with 5.1- by 5.1- by 0.63-cm angle iron. The metal ducts were made of 20-gauge galvanized sheet steel reinforced with angle iron. The ductwork was 0.61 by 0.61 m square except for those locations where transitions were used and the flow rate was measured.

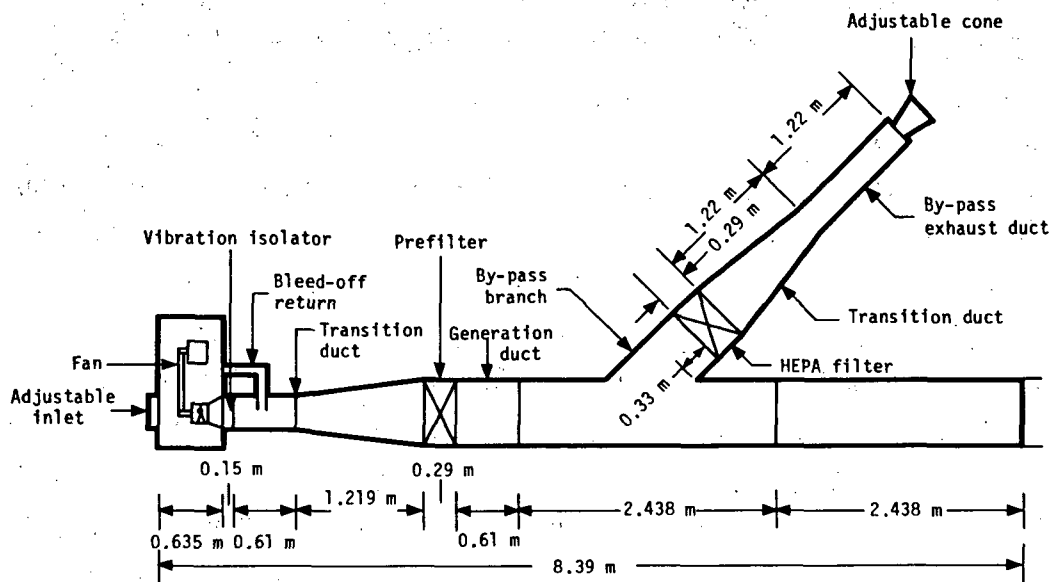


Fig. 1.  
Wind tunnel system - upstream section (plan view).

The fan was an axial-vane type manufactured by the Joy Corporation. The nominal rated airflow was  $4080 \text{ m}^3/\text{h}$  and was driven by a 5.7-kW Dyna Corporation electric motor operating at 1720 rpm. The fan assembly was enclosed in a wood box with an adjustable door that served as a variable inlet. The air flowing into the box first was cleaned by a furnace filter and subsequently was cleaned by a HEPA filter (prefilter) downstream from the fan in the duct. All transitions were gradual in their geometric configuration; the wall angles measured from the horizontal centerline were all less than  $7^\circ$ .

Immediately downstream from the HEPA filter prefilter, 2.4 m of stainless-steel duct was installed to facilitate addition of the test fuel burner or combustor. At the downstream edge of this steel duct, a turbulence mixing grid was added to disperse the combustion products over the duct airflow. The grid was composed of 2.2-cm-o.d. copper tubing spaced approximately 5.08 cm apart center to center. Furthermore, steady-state conditions prevailed in the duct within 1 min.

A Dwyer inclined manometer capable of a 0.005-cm-w.g. resolution was used to measure the centerline velocity pressure sensed by a pitot-static probe in the circular cross-section duct downstream from the HEPA filter test section. Horizontal and vertical traverses across the circular duct yielded velocity profiles that were used to calculate the volumetric airflow rate. A centerline

coefficient that relates the volumetric airflow rate to the centerline velocity then was determined. Repeating these calculations for the volumetric flows expected in a typical HEPA filter plugging test then relates the centerline velocity of volumetric airflow rate. Figure 2 shows the centerline coefficient as a function of volumetric flow where the coefficient is seen to vary slightly over the tested flows. The equation shown in Fig. 2 giving the centerline coefficient was used to determine all the volumetric airflows.

Air temperature measurements were made at five positions. The inlet and outlet dry and wet bulb temperatures were measured with a psychrometer. Copper-constantan (type T) thermocouples were used to measure the temperature of the airflow at the branch section upstream and downstream of the HEPA filter and the ambient temperature. A Series 2000 Thermocouple Digital Temperature Indicator was used to monitor the thermocouples, which were accurate to  $\pm 0.5^\circ\text{C}$  at the 95% confidence level.

### B. Test Fuel Combustion

The test fuels, PS and PMMA, were burned in a special solid fuel combustor designed by PNL. Figure 3 is an assembly drawing of the combustor. The burner was positioned on the underside of the stainless-steel duct immediately downstream from the HEPA prefilter and secured by a flanged steel pipe section using eight 0.79-cm-diam bolts.

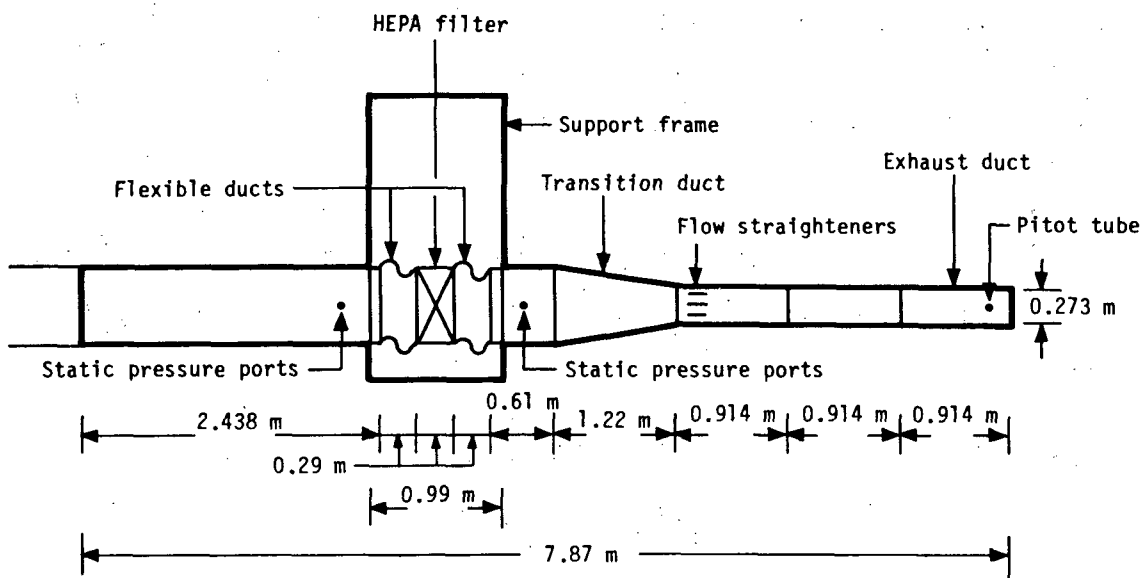


Fig. 2.  
Wind tunnel system - downstream section (plan view).

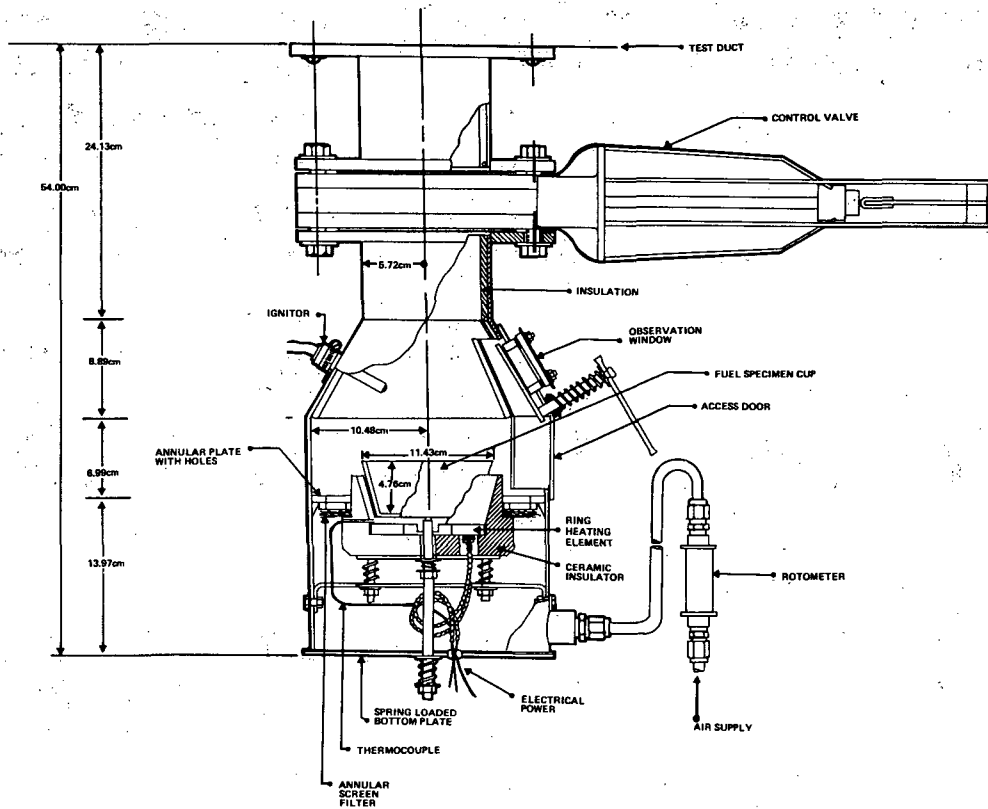


Fig. 3.  
 Assembly drawing of the test fuel combustor.

The combustor includes a cup holder where the fuel was contained and heated. The chamber walls provide the capability for combustion in a positive pressure atmosphere (duct interior). Fuel preheat temperatures were nominally 500°C and were achieved using a 400-W electrical ring heater controlled by a Chromalox on-off temperature controller. The flame was diffusion controlled, and the burning rate was regulated by adjusting the airflow rate to the combustor by means of a valve and rotameter. A gate valve at the top of the burner (under the stainless-steel duct) was maintained in the full-open position after the fire was started.

### C. Combustion Product Characterization

The characterization of the combustion products included only the particulate constituents. The particulate products were not monitored continuously, but rather intermittent samples were taken and analyzed.

Particulate mass concentrations (milligrams per cubic meter) were determined with Anderson Mark III stainless-steel in-stack inertial impactors incorporating straight nozzles. These impactors also measure aerodynamic particle diameter (based on unit density spheres) through seven stages of particle collection and a back-up filter. Pre-impactors for use in conjunction with the impactors were determined unnecessary for this application. Real-time particle sizing equipment also was used. The units used here were a Royco Model 225 Optical Aerosol Particle Counter and a Thermal Systems Model 3030 Electrical Mobility Analyzer. The real-time equipment was less suitable in this experiment because the particle size characteristics and mass concentration varied with the burn time. Because about 1--3 min of cycling time was required by each particle counter, the actual aerosol characteristics could not be resolved. In contrast, the inertial impactors were operated in such a manner (nozzle diameter and sampling time) to sample over the entire fuel burn--up to 20 min. For this reason, the impactor size data are considered pertinent to the duct wall particle deposition problem.

#### D. Smoke Deposition Measurement

The duct wall particulate mass deposition rate was measured approximately 1 hydraulic duct diameter upstream from the HEPA filter. The technique employed used a Nuclepore filter (polycarbonate, 0.03  $\mu\text{m}$  and 47 mm in diameter) secured to a specially designed back plate. The Nuclepore filter was kept in place by a ring of brass shim-stock that in turn was held onto the back plate by a vacuum as seen in Fig. 4. A drawback of this technique is the possibility for air leaks around the edge of the shim-stock that would necessarily alter the particulate deposition onto the Nuclepore filter. This potential problem was not resolved fully in this investigation. The gravimetric weight gain of the Nuclepore filter indicated the quantity of particulate deposition. A Sartorius Model 2007 Automatic Analytical Balance capable of mass resolutions of 0.1 mg was used in all the gravimetric analyses. We performed this wall deposition study to estimate the quantity of particle loss by transport within the duct.

#### IV. EXPERIMENTAL PROCEDURES

The systematic procedures associated with our smoke transport and deposition experiments are outlined below.

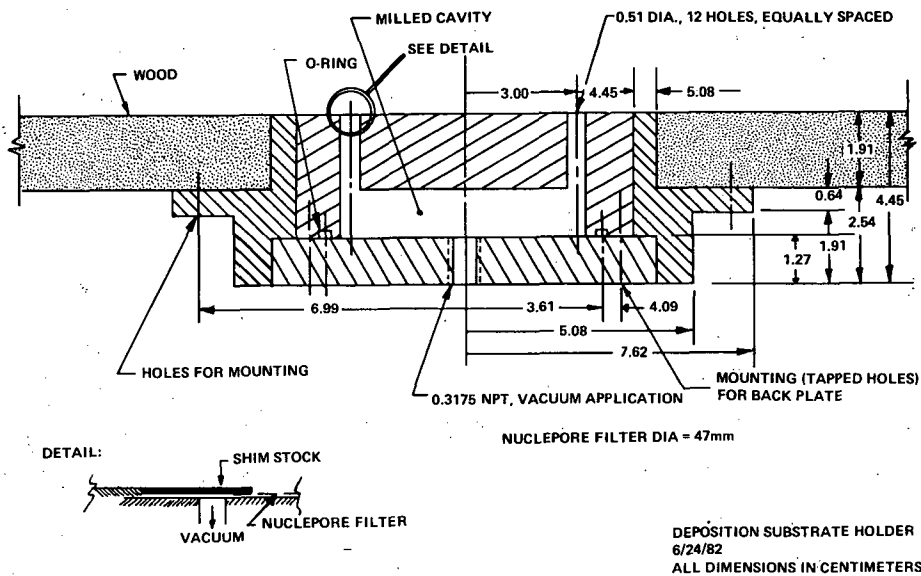


Fig. 4.  
Assembly drawing of the deposition substrate holder.

1. The test fuel cups were weighed when empty and when loaded with the PS fuel sample such that the mass was known for determination of the apparent burning rate. These cups next were placed on a hot plate with the temperature automatically controlled to 500°C.
2. All substrates were preweighed (Nuclepore filters for the deposition sites and the specially cut glass fiber filters for the inertial impactors) on an analytical balance, and the impactors were loaded.
3. The deposition substrates and impactors were transported to the air-flow facility and installed.
4. The test fuel cup ring heater within the combustor was switched on, and the Chromolox on-off controller was adjusted to 500°C. Approximately 40 min were required for the cup to achieve the set temperature. During this time, the fan prefilter was changed, all electronic instruments were rechecked, and the pressure manometers were adjusted for correct zeros.
5. The airflow facility fan was turned on.
6. Barometric pressure was recorded and corrected to temperature and local elevation.

7. The airflow-adjusting door located at the fan box was adjusted to yield the desired velocity pressure (volumetric airflow) measured in the circular cross-section duct downstream from the test HEPA filter.
8. Temperatures at the inlet, at the branch (downstream from combustor), upstream from the test HEPA filter, downstream from the HEPA filter, and at the exit were recorded. The static pressure drop across the filters also was recorded.
9. Impactor sampling at near isokinetic conditions was performed and then test fuel combustion was initiated.
10. The airflow facility fan was turned off to start the fire. The fuel test cup was placed inside the combustor in the cup holder, and the top gate valve was opened slightly. No air was supplied to the combustor, which allowed vapors to accumulate in the volume above the cup. After 5—10 min, the igniter coil was energized electrically. (Fuel vapor ignition occurred most consistently in this manner.) After combustion was initiated, the top gate valve was changed to full open and the combustion airflow adjusted to the required level ( $4.7 \times 10^{-4}$  or  $18.9 \times 10^{-4} \text{ m}^3/\text{s}$ ) on the rotameter by means of a valve.
11. The airflow facility fan was switched on. Thermocouple temperature measurements were recorded.
12. The data acquisition process involved the following items.
  - The time at which the flame first appeared was recorded.
  - The time at which the flame disappeared was recorded.
  - After flame disappearance, the top gate valve was closed and the inlet and exit dry and wet bulb temperatures and velocity pressure in the circular cross-section duct were recorded.
13. When all the test fuel was consumed, the airflow facility fan was turned off. Next, the impactors were shut down and removed. Finally, the deposition substrates were removed and placed in plastic petri dishes for transport back to the laboratory.
14. All substrates were final weighed on the analytical balance, and the measurements were recorded. The inertial impactors were washed and readied for the next test.

## V. TEST RESULTS AND DISCUSSION

### A. Physical Characterization of Smoke Particles

With the procedures given in the earlier section and with special instrumentation, the PS and PMMA combustion aerosols were characterized physically during the particulate deposition tests. Results were obtained from the inertial impactors located at the duct centerline--one approximately 4.9 m downstream from the burner and the second immediately upstream from the test HEPA filter. The distance between the impactors was 13.9 m. The impactors provided both overall particle mass concentration and size distribution by equivalent aerodynamic diameter. The purpose of the two simultaneous measurements was to determine the amount of reduction of airborne particulate mass as a result of duct wall deposition and the change in aerosol concentration.

The PS particle size distributions are shown in Fig. 5. The particulate mass concentration data, in conjunction with the mass burning rate, imply an important feature associated with PS combustion. This feature is that the total particulate mass concentration measured near the HEPA filter is proportional to the mass burning rate. This is established by ratioing the average high burning rate to the average low burning rate and obtaining the value of 2.0. Calculating the corresponding ratio for average total particulate mass concentrations gives 2.3. The correspondence (deviation from mean less than 7%) implies a constant soot fraction for under-ventilated conditions. Figure 5 also shows that the particle size distribution is nearly the same for particles less than  $2.0 \mu\text{m}$  for the high and low mass burning rates. However, for particles greater than  $2.0 \mu\text{m}$  in diameter, there is a significantly greater relative number of particles at the higher burning rate compared with the lower burning rate. Additionally, the aerodynamic mean particle diameter varies from about  $1.5$  to  $2.5 \mu\text{m}$  as seen in Fig. 5.

The corresponding particle size data for PMMA is shown in Fig. 6 as obtained from the impactors. In contrast to the PS combustion data, the ratios obtained for the fuel burning rates (under-ventilated divided by over-ventilated) and the downstream particulate mass concentrations are 1.0 and 3.6, respectively. There, with PMMA combustion at these different combustion conditions, the soot fraction is not constant. Further examination of Fig. 6 does not reveal any discernible features regarding the size distribution other than the mean aerodynamic diameter, which is significantly smaller than that of PS combustion (about  $0.7$  to  $1.0 \mu\text{m}$ ).

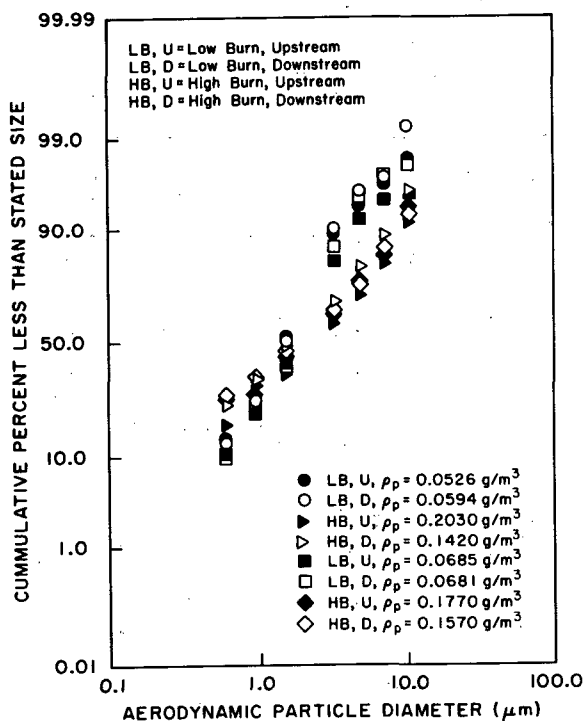


Fig. 5.  
Polystyrene combustion smoke  
particle size distribution.

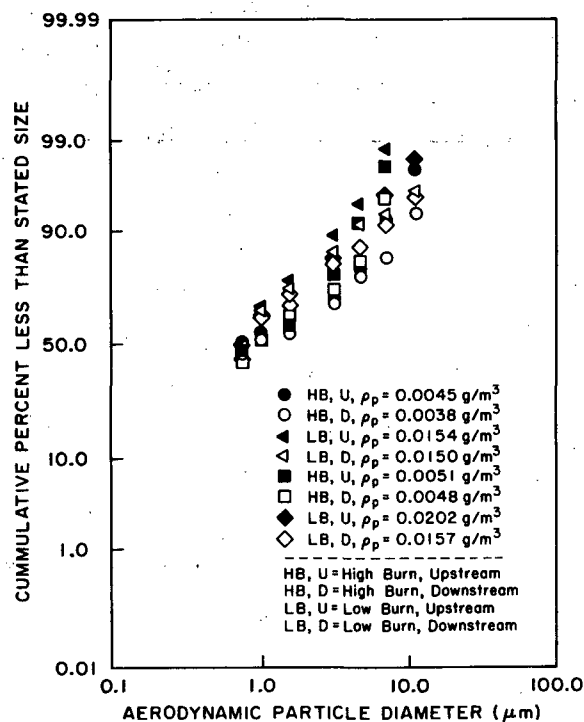


Fig. 6.  
Polymethyl methacrylate combustion  
smoke particle size distribution.

The effect of the 13.9-m transport length on duct centerline particulate mass concentration is summarized in Table II. The last two columns provided the calculation for  $\rho_p/\rho_{p0}$ , the particulate mass concentration ratio at the two impactors, for the experiments and the theory based on only gravitational settling [Eq. (17)]. Note that the averages of each of the four conditions are predicted by the theory with an error of less than 10% (based on averages) with the exception of the PS low burning rate condition, where the experimental result should be rejected.

Going back to Fig. 5, the change in particle size with transport along the 13.9-m length can be observed. With the exception of the larger (greater than 2.0  $\mu\text{m}$ ) particles, no clear shift in size distribution occurs. However, with these PS particles, the upstream size distribution by aerodynamic diameter relative to the corresponding downstream data of the same test suggests an average particle size reduction of about 1  $\mu\text{m}$ .

TABLE II  
 VARIATION OF PARTICULATE MASS CONCENTRATION BY TRANSPORT<sup>a</sup>

Fuel	Combustion Condition	Mass Concentration $\rho_{po}$ (g/m <sup>3</sup> )	Mass Concentration $\rho_{po}$ (g/m <sup>3</sup> )	$\left(\frac{\rho_p}{\rho_{po}}\right)_{exp.}$	$\left(\frac{\rho_p}{\rho_{po}}\right)_{theo.}$
PS	high	0.2027	0.1415	0.70	0.81
PS	high	0.1765	0.1566	0.89	0.89
PS	low	0.0526	0.0594	1.13	0.83
PS	low	0.0685	0.0681	0.99	0.84
PMMA	over-ventilated	0.0045	0.0038	0.84	0.89
PMMA	over-ventilated	0.0051	0.0048	0.94	0.75
PMMA	over-ventilated	0.0154	0.0150	0.97	0.75
PMMA	over-ventilated	0.0202	0.0157	0.78	0.86

<sup>a</sup>Duct length (from impactor-to-impactor) was 13.9 m.

Figures 7 and 8 show the volumes of soot particles generated by the burner for the two fuels as measured by an optical particle counter (Royco Model 225/518). The main features to note are the large variations of soot particle

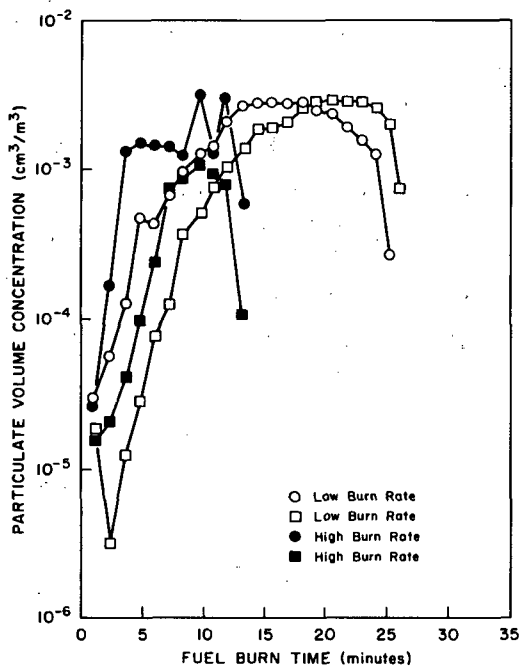


Fig. 7.  
 Variation of particulate volume concentration for polystyrene combustion smoke during fuel sample burns.

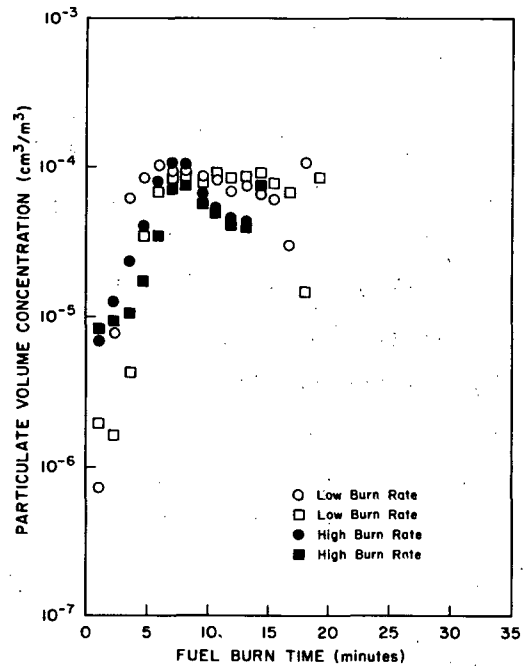


Fig. 8.  
 Variation of particulate volume concentration for polymethyl methacrylate combustion smoke during fuel sample burns.

output rates and the variation from burn to burn under the same conditions. Additionally, peak volumetric output rates for the PS and PMMA fuels vary by more than an order of magnitude.

### B. Smoke Particle Wall Deposition

Table III summarizes the numerical data obtained during the duct wall deposition tests. In these tests, the accumulated particulate mass on the HEPA filters and the actual particulate mass deposits at the duct wall were measured in addition to the physical characteristics of the airborne particles as already described. The values reported for the duct volumetric flow rate are arithmetic averages of the flow at the initiation and conclusion of each test.

First, the experimental deposition results are given in Table IV. The important operational conditions are given in order to identify each test. Under the columns labeled as "Experimental Data," the experimental results alone are presented where the final result is a particulate mass ratio,  $m_d/m_b$ , and is the mass deposited on duct walls divided by the mass of unburned fuel. The mass deposited on the walls,  $m_d$ , is given by

$$m_d = Y_s m_b - m_f \quad , \quad (18)$$

where  $m_f$  is the accumulated particulate mass on the HEPA filter for the fuel burned. This ratio identifies that portion of the fuel mass that was deposited on the walls. This calculation assumes the appropriate constant value of  $Y_s$  (0.33 for PS and 0.021 for PMMA) regardless of the burning condition. This experimental mass-balance technique was not sufficiently sensitive to discern wall mass deposition at the under-ventilated PMMA burn rate.

Applying the gravitational settling theory requires calculating two variables related to the combustion particles. These are the particle settling velocity,  $u_{ps}$ , and the upstream particulate mass concentration,  $\rho_{pob}$ , at the burner. Because the quantity  $m_p J_p$  is the particulate mass flux, using Eq. (1) gives

$$u_{ps} = \frac{m_p J_p}{m_p n_p} = \frac{m_p J_p}{\rho_p} \quad , \quad (19)$$

TABLE III  
DUCT WALL DEPOSITION EXPERIMENTAL DATA

Fuel Type	Burn Condition	Fuel Mass burned (g)	Total Test Time (min)	Fuel Mass Burn Rate, $\frac{g}{min}$	Volumetric Duct Airflow Rate Q ( $m^3/h$ )	Upstream Impactor Conc. $\frac{g}{m}$	Downstream Impactor Conc. $\frac{g}{m}$	Accumulated HEPA Mass Gain (g)	Wall Nuclepore Mass Deposit (mg)		
									Filter Top	Side	Bottom
PS	1.7 $m^3/h$ Combustion Air Low Burn Rate, Underventilated	200.7	21.9	9.16	1642	0.0526	0.0594	14.76	0.2	0.2	1.1
PS	1.7 $m^3/h$ Combustion Air Low Burn Rate, Underventilated	250.0	29.7	8.96	1470	0.0685	0.0681	32.3	0.1	0.1	0.8
PS	6.8 $m^3/h$ Combustion Air High Burn Rate, Underventilated	250.0	14.35	17.42	1589	0.2027	0.1415	71.02	0.2	0.3	1.5
PS	6.8 $m^3/h$ Combustion Air High Burn Rate, Underventilated	250.3	13.60	18.40	1439	0.1765	0.1566	65.0	0.2	0.4	1.4
PMMA	3.4 $m^3/h$ Combustion Air Low Burn Rate, Underventilated	600.5	50.1	12.0	1607	0.0154	0.0150	22.9	0.1	0.1	0.4
PMMA	3.4 $m^3/h$ Combustion Air Low Burn Rate, Underventilated	600.0	52.4	11.48	1448	0.0202	0.0157	13.0	0.0	0.1	0.8
PMMA	8.5 $m^3/h$ Combustion Air High Burn Rate, Overventilated	1000.3	81.9	12.26	1700	0.0045	0.0038	5.43	0.1	0.1	0.4
PMMA	8.5 $m^3/h$ Combustion Air High Burn Rate, Overventilated	1000.0	85.6	11.70	1530	0.0051	0.0048	5.64	0.0	0.1	0.3

TABLE IV  
EXPERIMENTAL DEPOSITION RESULTS USING GRAVITATIONAL SETTLING THEORY

Fuel Type	Burn Condition	Fuel Mass Burned, $m_b$ (g)	$\left(\frac{m_p J_p}{gm^2 h}\right)$	$U_{ps}$ $\frac{m}{h}$	$\left(\frac{\rho_{poc}}{g/m^3}\right)$	Gravitational Settling Theory				Apparent Soot Fraction $y_{sa}$	Experimental Data		
						Accumulated HEPA Mass Gain, $m_f$ (g)	$m_{dg}$	$\frac{m_{dg}}{m_b}$	Total Mass Accounted (g)		$m_b y_s$	$m_d = y_s m_b - m_f$	$\frac{m_d}{m_b}$
PS	Low	200.7	2.66	44.8	$1.10 \times 10^{-1}$	14.8	17.8	0.0887	32.6	0.16	66.2	51.4	0.256
PS	Low	250.0	1.43	21.0	$1.21 \times 10^{-1}$	32.3	13.4	0.0536	45.7	0.18	82.5	50.2	0.201
PS	High	250.0	5.53	39.1	$2.17 \times 10^{-1}$	71.0	20.4	0.0816	91.4	0.37	82.5	11.5	0.046
PS	High	250.3	5.44	34.7	$2.53 \times 10^{-1}$	65.0	20.0	0.0799	85.0	0.34	82.6	17.6	0.070
PMMA	Low	600.5	0.422	28.1	$9.42 \times 10^{-3}$	22.9	2.31	0.00385	25.2	0.042	12.6	-10.3	
PMMA	Low	600.0	0.808	51.5	$9.96 \times 10^{-3}$	13.0	4.24	0.00707	17.2	0.029	12.6	-0.4	
PMMA	High	1000.3	0.258	67.9	$9.06 \times 10^{-3}$	5.43	7.76	0.00776	13.2	0.013	21.0	15.6	0.0156
PMMA	High	1000.0	0.185	38.5	$9.66 \times 10^{-3}$	5.64	5.21	0.00531	11.0	0.011	21.0	15.4	0.0154

where  $\rho_p$  is the duct centerline particulate mass concentration and was measured at the downstream impactor. The particulate mass wall flux also was measured at the downstream impactor, and thus the  $u_{ps}$  calculated here is the downstream value. In this analysis, the  $u_{ps}$  values are assumed to be constant over the duct length. Values of  $u_{ps}$  on the mean aerodynamic particle diameter as determined by the impactors are on the order of 1 m/m or less for the two fuels. Because these values for  $u_{ps}$  do not reflect the realistic values shown in Table IV as determined above, the mean aerodynamic particle diameter was not used and thus not recommended for particle deposition calculations associated with combustion aerosols.

The second variable,  $\rho_{pob}$ , is obtained from

$$\rho_{pob} = \frac{m_b y_s}{Q}, \quad (20)$$

where  $Q$  is the duct volumetric airflow rate (cubic meters per hour). Finally, modifying Eq. (14) gives the particulate mass deposit considering only gravitational settling:

$$m_{dg} = \rho_{pob} Q \left[ 1 - e^{-\left(\frac{u_{ps} L}{U_h}\right)} \right] \Delta t, \quad (21)$$

where  $L$  is the straight duct length between the burner and downstream impactor (19.63 m) and  $\Delta t$  is the test duration (in hours). The results from Eq. (21) and the mass ratio  $m_{dg}/m_b$  are given in Table IV.

Comparing the predicted and experimental PS combustion aerosol deposition quantities suggests that, within a factor of 2 or 3, the values of  $m_{dg}/m_b$  agree. This level of agreement weakly supports the gravitational settling theory. Additionally, the calculated or apparent PS soot fraction,  $Y_{sa}$ , is within 12% of the 0.33 value at the high burn rate tests, thus indicating the correctness of  $Y_s$  for the PS fuel at these conditions. For the low burn rate conditions, the  $Y_{sa}$  values are significantly lower than the assumed  $Y_s$  value of 0.33. Already argued is the consistency of  $Y_s$  based on the fuel mass burn rates and

downstream particle concentrations. Consequently, the gravitational settling theory underestimates the mass deposit for the PS low burn rate conditions. With the PMMA tests, comparisons can be made only for the over-ventilated combustion condition;  $m_d$  is negative for the under-ventilated conditions. Again, the mass ratios and soot fractions agree to a factor of 3 or less. However, the consistency of  $Y_{sa}$  data suggests that  $Y_s$  is indeed different for the two conditions--by a factor of at least 2 for these experiments.

Gravitational settling is accompanied by other deposition mechanisms in a horizontal duct and include turbulent diffusion, inertial impaction, and electrostatic effects. For the horizontal straight duct used in these experiments, inertial and electrostatic effects were not significant.\* To use the wall particulate mass flux measurements made in the vertical and top walls of the duct at the downstream impactor, an expression for the deposited particulate mass flux by turbulent diffusion must be developed regarding the flux measurements made. Rewriting Eq. (6) and incorporating the four sides of the duct (bottom, top, and two sides), we have

$$J_p = n_{p_{i=1}} \sum_{i=1}^4 k_{pi} = (2K_{ps} + k_{pt} + k_{pl}) n_p \quad (22)$$

where  $k_p$  is the particle mass transfer coefficient for turbulent diffusion (centimeters per second) and the subscripts s, t, and l refer to the sides, top, and lower surface, respectively. Proceeding as before with gravitational settling alone, the downstream to upstream particle number concentration ratio assuming constant  $k_{pi}$  is

$$\frac{n_p}{n_{p0}} = e^{-x/U \left[ \frac{2K_{ps}}{w} + \frac{k_{pt} + k_{pl}}{h} \right]} \quad (23)$$

\*For long and complex duct geometrics, both particle inertial and electrostatic effects are likely important.

and after integration over the duct area, the particulate mass deposit is given by

$$m_{dt} = \rho_{po} Q \left[ 4 - 2e^{-\frac{k_{ps}L}{wU}} - e^{-\frac{-k_{pt}L}{hU}} - e^{-\frac{-k_{ps}L}{hU}} \right] \Delta t \quad (24)$$

resulting only from turbulent diffusion.

Table V summarizes the results of the particulate deposition experiments adding turbulent diffusion to the gravitational settling calculation. In these calculations, the mass flux measured at the duct bottom wall is separated into two parts—gravitational settling and turbulent diffusion. The diffusion portion is determined roughly by averaging the side and top particulate mass flux deposition rates. The gravitational portion then is assumed as the remainder. In Table V, the values of  $k_{pi}$  are calculated from the particulate flux measurements as

$$k_{pi} = \frac{m_{pi} J_{pi}}{\rho_p} \quad (25)$$

for a specific wall of the duct. Under the heading "Theoretical Prediction," the values resulting from the sum of gravitational and diffusion deposition are given. With the consideration of these two mechanisms, the PS deposition tests indicate that the theory underestimates for the low burn rate and overestimates for the high burn rate total duct wall deposit. With PMMA tests, the combined theory does fairly well in that agreement is within 50%. Additionally, gravitational settling alone (corrected for diffusion) predicts the actual deposit to within 15% of the PS high burn rate data. However, the PS low burn rate deposition data remains unexplained.

In any event, the deposition rates predicted by theory are not fully embraced by the experimental data. Two reasons for this are the preliminary and thus relatively crude nature of the particle deposition experiments and the simplistic theoretical model used at present in FIRAC. Additionally, because the mean particle diameters determined by the impactors are much too small, the

TABLE V  
EXPERIMENTAL DEPOSITION RESULTS USING TURBULENT DIFFUSION AND GRAVITATIONAL SETTLING THEORY

Fuel Type	Burn Condition	Fuel Mass Burned, $m_b$ (g)	Gravitational Settling					Turbulent Diffusion							
			Bottom Wall Nuclepore Filter Mass Deposit for Only Gravitational Settling (mg)	$\frac{m_{pp}}{m^2 h}$	$\frac{U_{ps}}{m/h}$	$\frac{\rho_{poc}}{m^3}$	$\frac{m_{dg}}{g}$	$\frac{k_{pv}}{m/h}$	$\frac{k_{pt}}{m/h}$	$\frac{k_{pb}}{m/h}$	$\frac{m_{dt}}{g}$	$\frac{m_d}{g}$	$\left(\frac{m_d}{m_b}\right)_{g+t}$	$\frac{m_d}{g}$	$\left(\frac{m_d}{m_b}\right)_{exp}$
PS	Low	200.7	0.9	2.17	36.5	$1.10 \times 10^{-1}$	14.9	8.13	8.13	8.13	14.6	29.5	0.14700	51.4	0.256
PS	Low	250.0	0.7	1.25	18.4	$1.21 \times 10^{-1}$	11.8	2.61	2.61	2.61	7.31	18.9	0.0756	50.2	0.201
PS	High	250.0	1.2	4.42	31.2	$2.17 \times 10^{-1}$	16.7	7.85	5.21	7.85	16.8	33.5	0.134	11.5	0.046
PS	High	250.3	1.1	4.27	27.3	$2.53 \times 10^{-1}$	16.2	9.96	4.97	7.47	20.7	36.9	0.147	17.6	0.070
PMMA	Low	600.5	0.3	0.317	21.1	$9.42 \times 10^{-3}$	1.78	7.07	7.07	7.07	2.50	4.28	0.00713		
PMMA	Low	600.0	0.7	0.0707	45.0	$9.96 \times 10^{-3}$	3.79	6.43	0.00	6.43	14.5	18.3	0.0305		
PMMA	High	1000.3	0.3	0.194	51.1	$9.06 \times 10^{-3}$	6.16	17.0	17.0	17.0	9.15	15.3	0.0153	15.6	0.0156
PMMA	High	1000.0	0.2	0.124	25.8	$9.66 \times 10^{-3}$	3.72	12.9	0.00	12.9	26.9	30.6	0.0306	15.4	0.0154

gravitational settling theory currently used in FIRAC is not conservative but rather significantly underpredicts the actual particulate mass deposition rates by the combustion aerosols tested. Successful particle deposition studies in which theory and experimental results are mutually supportive will require improved theoretical developments incorporating additional deposition mechanisms and improved experimental techniques and procedures.

#### IV. CONCLUSIONS AND RECOMMENDATIONS

We developed the following conclusions from experimental work involving the combustion products of PS and PMMA fuel:

1. Particulate mass deposition is an important feature associated with the flow of combustion products and, even for short duct lengths (31 hydraulic diameters), may reach 25% of the unburned fuel as with PS.
2. Physical changes associated with the transport of the particulate combustion products include a 10 to 30% reduction in mass concentration and a small ( $\approx 1\text{-}\mu\text{m}$ ) reduction in particle size only observable for the PS combustion particles with an aerodynamic diameter greater than  $2.0\ \mu\text{m}$ .
3. Comparisons of the experimental results with the theory incorporating gravitational settling provide some checks but cannot be considered supportive. Extending the theory to include turbulent diffusion and gravitational settling provides improvement for one experimental condition—over-ventilated PMMA combustion—but worsens the agreement for the high PS burn rate condition.
4. The experimental techniques used in this effort are not sufficiently sensitive to verify the deposition models described.

Because HEPA filter plugging rates and efficiencies depend on the airborne particulate mass and size distributions arriving at the filter, deposition is an important consideration. The experimental work performed here establishes some support for the theory developed and used in FIRAC. However, improved experiments directed at the deposition problem alone are required to establish the important deposition mechanisms that should be included in the FIRAC code.

## ACKNOWLEDGMENT

The authors acknowledge the assistance of M. V. Gunaji of NMSU who operated the PNL compustor, ran the test facility, and made numerous measurements.

## REFERENCES

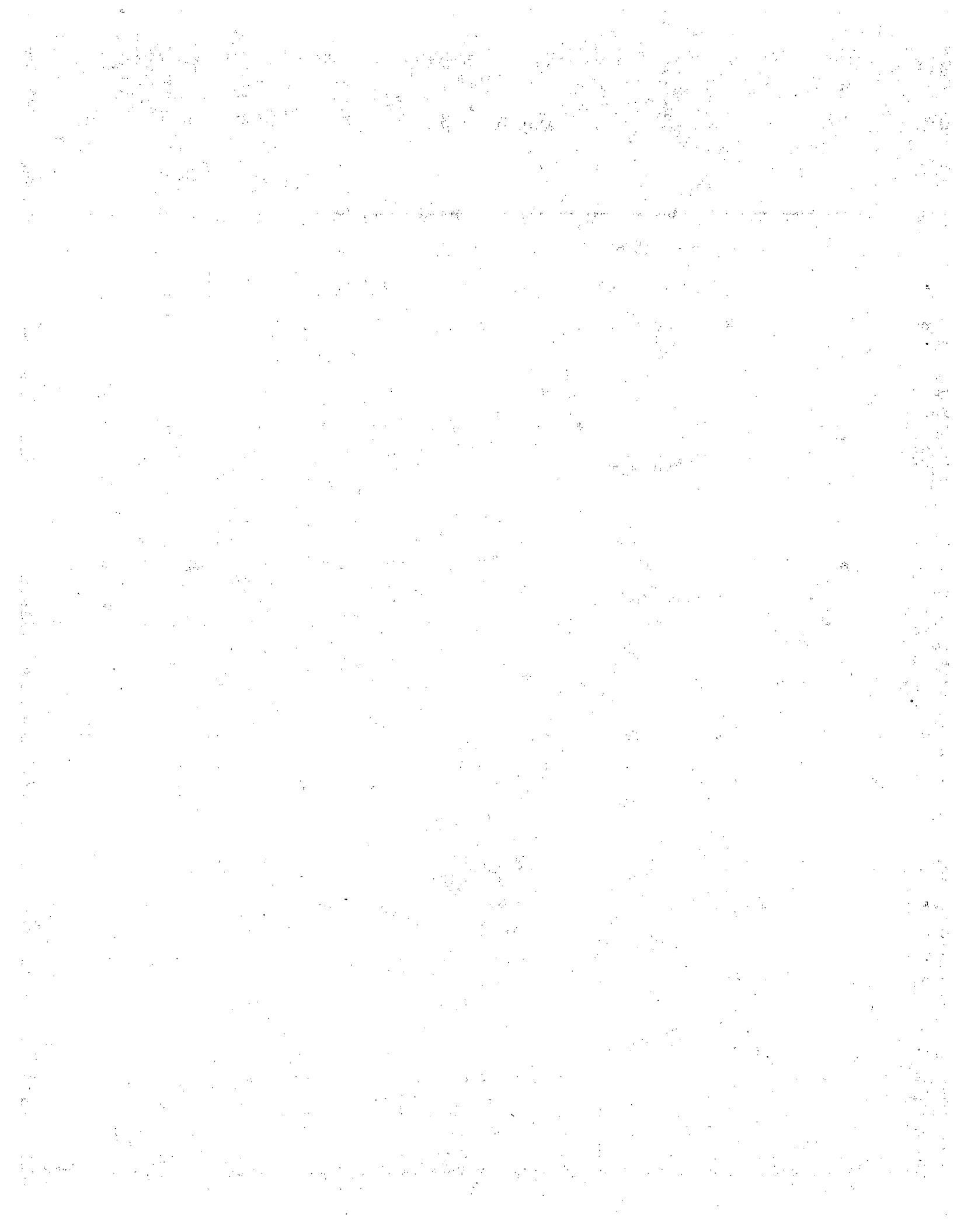
1. R. W. Andrae, J. W. Bolstad, W. S. Gregory, F. R. Krause, R. A. Martin, P. K. Tang, M. Y. Ballinger, M. K. W. Chan, J. A. Glissmeyer, P. C. Owczarski, J. Mishima, S. L. Sutter, E. L. Compere, H. W. Godbee, and S. Bernstein, "Methods for Nuclear Air Cleaning System Accident Consequence Assessment," in Proc. of 17th DOE Nuclear Air Cleaning Conference, US Department of Energy report CONF-820833 (February 1983).
2. "Fuel Cycle Facility Accident Analysis Handbook," Los Alamos National Laboratory report LA-9180-M, NUREG/CR-2508, PNL-4149 (in preparation).
3. R. W. Andrae, J. W. Bolstad, W. S. Gregory, F. R. Krause, R. A. Martin, and P. K. Tang, "FIRAC Users Manual - A Computer Code for Analysis of Fire-Induced Flow and Material Transport in Nuclear Facilities," Los Alamos National Laboratory report (in preparation).
4. R. A. Martin, P. K. Tang, A. P. Harper, J. D. Novat, and W. S. Gregory, "Material Transport Analysis for Accident-Induced Flow in Nuclear Facilities," Los Alamos National Laboratory report LA-9913-MS, NUREG/CR-3527 (October 1983).
5. P. K. Tang, "Material Convection Model," Los Alamos National Laboratory report LA-9393-MS (June 1982).
6. N. Alvares, D. Beason, V. Bergman, J. Creighton, H. Ford, and A. Lipska, "Fire Protection Countermeasures for Containment Ventilation," Lawrence Livermore National Laboratory Progress report UCID-18781 (September 1980).
7. W. S. Gregory, R. A. Martin, P. R. Smith, and D. E. Fenton, "Response of HEPA Filters to Simulated Accident Conditions," in Proc. of the 17th DOE Nuclear Air Cleaning Conference, US Department of Energy report CONF-820833 (February 1983).
8. D. L. Fenton, J. J. Dallman, P. R. Smith, R. A. Martin and W. S. Gregory, "The Los Alamos National Laboratory/New Mexico State University Filter Plugging Test Facility--Description and Preliminary Test Results," Los Alamos National Laboratory report LA-9929-MS, NUREG/CR-3242 (October 1983).
9. D. L. Fenton, W. S. Gregory, M. V. Gunaji, and P. K. Tang, "Combustion Aerosol Plugging of High-Efficiency Particulate Air Filters," Los Alamos National Laboratory report (in preparation).
10. W. Bergman, H. Hebard, R. Taylor, and B. Lum, "Electrostatic Filters Generated by Electric Fields," Lawrence Livermore Laboratory paper UCRL-81926 (July 1979), submitted to Second World Filtration Congress (London, September 18--20, 1979).

11. F. R. Krause and W. S. Gregory, "Simulation of Forced Ventilation Fires," in Proc. of the 17th DOE Nuclear Air Cleaning Conference, US Department of Energy report CONF-820833 (February 1983).
12. J. J. Dallman, "HEPA Filter Loading by Simulated Combustion Products," Masters Thesis submitted to Mechanical Engineering Department, New Mexico State University (Las Cruces, New Mexico, 1982).
13. A. Tewarson, "Physico-Chemical and Combustion Pyrolysis Properties of Polymeric Materials," Factory Mutual Research Corp. Technical Report FMRC J. I. OEON6.RC/RC80-T-79 (November 1980).
14. S. H. Friedlander, Smoke, Dust and Haze (John Wiley and Sons, New York, 1977).
15. N. A. Fuchs, The Mechanics of Aerosols (Pergamon Press Ltd., Oxford, 1964).
16. S. L. Soo, Fluid Dynamics of Multiphase Systems (Blaisdell Publishing Company, Waltham, Massachusetts, 1967).
17. C. N. Davies, Ed., Aerosol Science (Academic Press, New York, 1966).
18. D. C. Kaul, Ed., "Adversary Actions in the Nuclear Power Fuel Cycles: Reference Events and Their Consequences, Volume IV., Consequence Assessment Methodology," Science Applications Inc. report SAI-152-123-80-1 (March 1981).
19. T. T. Mercer, Aerosol Technology in Hazard Evaluation (Academic Press, New York, 1973).
20. R. Dennis, "Handbook on Aerosols," Technical Information Center, Energy Research and Development Administration report TID-26608 (1978).
21. S. K. Friedlander and H. F. Johnstone, "Deposition of Suspended Particles from Turbulent Gas Streams," Ind. Engn. Chem. 49, 1151 (1957).
22. B. Y. H. Liu and J. K. Agarwal, "Experimental Observation of Aerosol Deposition in Turbulent Flow," J. Aerosol Sci. 5, 145 (1974).
23. S. K. Beal, "Deposition of Particles in Turbulent Flow on Channel or Pipe Walls," Nucl. Sci. Engng. 40, 1 (1970).
24. C. S. Lin, R. W. Moulton, and G. L. Putnam, "Mass Transfer Between Solid Wall and Fluid Streams," Ind. Engng. Chem. 45, 636 (1953).
25. H. Matsui, Y. Yoshida, M. Murata, and T. Okata, "Measurement of Deposition Fraction of Aerosol Particles in a Horizontal Straight Metal Pipe," J. Nucl. Sci. and Tech. 11, 26 (1974).
26. R. W. Andrae, P. K. Tang, R. A. Martin, and W. S. Gregory, "TORAC User's Manual - A Computer Code for Analysis of Tornado-Induced Flow and Material Transport in Nuclear Facilities," Los Alamos National Laboratory report (in preparation).

27. P. K. Tang, R. W. Andrae, J. W. Bolstad, R. A. Martin, and W. S. Gregory, "EXPAC Users Manual - A Computer Code for Analysis of Explosion-Induced Flow and Material Transport in Nuclear Facilities," Los Alamos National Laboratory report (in preparation).
28. H. E. Hesketh, Fine Particles in Gaseous Media (Ann Arbor Science Publishers, Inc., Ann Arbor, Michigan, 1977).

DISTRIBUTION

	<u>Copies</u>
Nuclear Regulatory Commission, RI, Laurel, Maryland	173
Technical Information Center, Oak Ridge, Tennessee	2
Los Alamos National Laboratory, Los Alamos, New Mexico	40
	<hr/> 215



NRC FORM 335 (2-84) NRCM 1102, 3201, 3202		U.S. NUCLEAR REGULATORY COMMISSION		1. REPORT NUMBER (Assigned by TIDC, add Vol. No., if any)	
<b>BIBLIOGRAPHIC DATA SHEET</b>				NUREG/CR-4321 LA-10478-MS	
SEE INSTRUCTIONS ON THE REVERSE				3. LEAVE BLANK	
2. TITLE AND SUBTITLE Full-Scale Measurements of Smoke Transport and Deposition in Ventilation System Ductwork				4. DATE REPORT COMPLETED	
5. AUTHOR(S) R. A. Martin and D. L. Fenton				MONTH: June      YEAR: 1985	
				6. DATE REPORT ISSUED	
7. PERFORMING ORGANIZATION NAME AND MAILING ADDRESS (Include Zip Code) Los Alamos National Laboratory Los Alamos, NM 87545				8. PROJECT/TASK/WORK UNIT NUMBER	
				9. FIN OR GRANT NUMBER A7029	
10. SPONSORING ORGANIZATION NAME AND MAILING ADDRESS (Include Zip Code) Division of Risk Analysis Office of Nuclear Regulatory Research U.S. Nuclear Regulatory Commission Washington, DC 20555				11a. TYPE OF REPORT Informal	
				b. PERIOD COVERED (Inclusive dates)	
12. SUPPLEMENTARY NOTES					
13. ABSTRACT (200 words or less) <p>This study is part of an effort to obtain experimental data in support of the fire accident analysis computer code FIRAC, which was developed at the Los Alamos National Laboratory. FIRAC can predict the transient movement of aerosolized or gaseous material throughout the complex ventilation systems of nuclear fuel cycle facilities. We conducted a preliminary set of full-scale material depletion/modification experiments to help assess the accuracy of the code's aerosol depletion model. Such tests were performed under realistic conditions using real combustion products in full-sized ducts at typical air-flow rates. To produce a combustion aerosol, we burned both polystyrene and polymethyl methacrylate, the most and least smoky fuels typically found in fuel cycle plants, under varied ventilation (oxygen-lean and oxygen-rich) conditions.</p> <p>Aerosol mass deposition, size, and concentration measurements were performed. We found that as much as ~25% of polystyrene smoke mass and as little as 2% of the polymethyl methacrylate generated at the entrance to a 15.2-m duct is deposited on the duct walls. We also compared our experimental results with theoretical equations currently used in FIRAC.</p>					
14. DOCUMENT ANALYSIS - a. KEYWORDS/DESCRIPTORS				15. AVAILABILITY STATEMENT Unlimited	
b. IDENTIFIERS/OPEN-ENDED TERMS				16. SECURITY CLASSIFICATION (This page) Unclassified	
				(This report) Unclassified	
				17. NUMBER OF PAGES	
				18. PRICE	